**Atmospheric
Chemistry
and Physics**

Flight-based chemical characterization of biomass burning aerosols within two prescribed burn smoke plumes

K. A. Pratt[1,2,*]**, S. M. Murphy**[3,4]**, R. Subramanian**[5]**, P. J. DeMott**[6]**, G. L. Kok**[5]**, T. Campos**[7]**, D. C. Rogers**[7]**,
A. J. Prenni**[6]**, A. J. Heymsfield**[7]**, J. H. Seinfeld**[3]**, and K. A. Prather**[1,8]

[1]Department of Chemistry and Biochemistry, University of California, San Diego, La Jolla, CA, USA
[2]Atmospheric Science and Global Change Division, Pacific Northwest National Laboratory, Richland, WA, USA
[3]Division of Chemistry and Chemical Engineering, California Institute of Technology, Pasadena, CA, USA
[4]Chemical Sciences Division, Earth System Research Laboratory, National Oceanic & Atmospheric Administration, Boulder,
CO, USA
[5]Droplet Measurement Technologies, Boulder, CO, USA
[6]Department of Atmospheric Science, Colorado State University, Fort Collins, CO, USA
[7]National Center for Atmospheric Research, Boulder, CO, USA
[8]Scripps Institution of Oceanography, University of California, San Diego, La Jolla, CA, USA
[*]now at: Department of Chemistry, Purdue University, West Lafayette, IN, USA

Abstract. Biomass burning represents a major global source of aerosols impacting direct radiative forcing and cloud properties. Thus, the goal of a number of current studies involves developing a better understanding of how the chemical composition and mixing state of biomass burning aerosols evolve during atmospheric aging processes. During the Ice in Clouds Experiment-Layer Clouds (ICE-L) in the fall of 2007, smoke plumes from two small Wyoming Bureau of Land Management prescribed burns were measured by on-line aerosol instrumentation aboard a C-130 aircraft, providing a detailed chemical characterization of the particles. After ~2–4 min of aging, submicron smoke particles, produced primarily from sagebrush combustion, consisted predominantly of organics by mass, but were comprised primarily of internal mixtures of organic carbon, elemental carbon, potassium chloride, and potassium sulfate. Significantly, the fresh biomass burning particles contained minor mass fractions of nitrate and sulfate, suggesting that hygroscopic material is incorporated very near or at the point of emission. The mass fractions of ammonium, sulfate, and nitrate increased with aging up to ~81–88 min and resulted in acidic particles. Decreasing black carbon mass concentrations occurred due to dilution of the plume. Increases in the fraction of oxygenated organic carbon and the presence of dicarboxylic acids, in particular, were observed with aging. Cloud condensation nuclei measurements suggested all particles >100 nm were active at 0.5 % water supersaturation in the smoke plumes, confirming the relatively high hygroscopicity of the freshly emitted particles. For immersion/condensation freezing, ice nuclei measurements at −32 °C suggested activation of ~0.03–0.07 % of the particles with diameters greater than 500 nm.

1 Introduction

Biomass burning emissions produce a considerable amount of greenhouse gases and are estimated to contribute ~34–38 % of global carbonaceous aerosol (Forster et al., 2007). Biomass burning aerosols exert a significant, but uncertain, direct radiative forcing of +0.03 [±0.12] W m^{-2}, which is strongly influenced by aerosol overlying clouds (Forster et al., 2007; Chand et al., 2009). Wildfires also serve as large sources of cloud condensation nuclei (CCN) with a wide range of hygroscopicities (Petters et al., 2009a; Carrico et al., 2010) and can also be a source of heterogeneous ice nuclei (IN) with number concentrations suggested to be of regional importance (Pueschel and Langer, 1973; Petters et al., 2009b; Twohy et al., 2010). Biomass burning aerosols have

been identified as having a significant anthropogenic component, and emissions are expected to increase further by a warming climate and land-use changes (Westerling et al., 2006; Forster et al., 2007; Spracklen et al., 2009). In the western United States, biomass burning contributes ∼50 % of the annual average total carbonaceous aerosol mass concentrations and ∼30 % of total fine aerosol mass concentrations (Park et al., 2007). Moreover, in the United States, large wildfire activity has increased in recent years with higher large-wildfire frequency, longer wildfire durations, and longer wildfire seasons, particularly in the mid-elevation northern Rocky Mountains (Westerling et al., 2006). Recent modeling by Spracklen et al. (2009) estimates an increase of 54 % in the annual mean area burned in the western United States from 2000 to 2050, corresponding to increases in summertime organic carbon (OC) and elemental carbon (EC) aerosol concentrations in the western United States of 30 % and 19 %, respectively.

Numerous studies have investigated the physical and chemical characteristics of biomass burning aerosols. In general, fresh dry smoke particles, primarily in the submicron size range, have been found to consist of ∼80 % OC, ∼5–9 % black carbon (BC), and ∼12–15 % trace inorganics, such as potassium, sulfate, chloride, and nitrate (Reid et al., 2005b). These individual particles are usually internally mixed with a core of black carbon and alkali earth compounds coated with organics (Reid et al., 2005b). Different fuels and combustion conditions produce particles of varying chemical composition, with potassium and soot enhanced in flaming combustion, for example (Reid et al., 2005b; Cahill et al., 2008). Following emission, particle growth is rapid with aged smoke becoming enriched in sulfate, nitrate, organic acids and semivolatile organic species (Gao et al., 2003; Reid et al., 2005b). Most chemical characterization studies have utilized filter-based thermal desorption methods to quantify OC and BC; however, these methods can suffer from sampling artifacts and uncertainties in evolution temperatures. Thus, quantification of organic carbon and black carbon from biomass burning was identified in a review by Reid et al. (2005b) as the greatest need in smoke particle chemistry research. A secondary recommendation by Reid et al. (2005b) was to investigate further the aging of smoke particles immediately following emission with high time resolution to bridge the gap between fresh and aged biomass burning aerosols, the physical and chemical properties of which impacts optical properties and cloud-forming potentials.

Most airborne plume studies, including recent measurements (Capes et al., 2008; Yokelson et al., 2009), have focused on large fires. Herein we examine two relatively small prescribed burns at low ambient temperatures. Prescribed fires provide the opportunity for a detailed characterization of both burn conditions and consequent emissions in a real-world setting, combining the advantages of studying wildfires and laboratory fires. In addition, prescribed fires may serve as a means to reduce CO_2 fire emissions in the western United States (Wiedinmyer and Hurteau, 2010). During the Ice in Clouds Experiment-Layer Clouds (ICE-L) in November 2007, the smoke plumes of two prescribed burns were intercepted during flights of the National Center for Atmospheric Research/ National Science Foundation (NSF/NCAR) C-130 aircraft. The young smoke plumes were investigated in detail utilizing a unique suite of real-time aerosol instrumentation, measuring single-particle chemical composition, non-refractory aerosol mass concentrations, and black carbon mass concentrations. Concurrent measurements of CCN and IN were also obtained and provide a basis for discussing aerosol cloud activation properties.

2 Experimental

2.1 Overview

Measurements within two Wyoming Bureau of Land Management (BLM) prescribed burn smoke plumes were made aboard the NSF/NCAR C-130 aircraft during ICE-L research flights #1 (RF01) and #3 (RF03) in November 2007. An overview of the prescribed burns and ground conditions, provided by the Wyoming BLM, is detailed in Table 1, presenting date, latitude, longitude, elevation, burn time, ambient temperature, relative humidity, wind speed, burn area, fuel types, and live fuel moisture. There was no surface snow cover in the vicinity of these burns. The flight procedure was as follows: when a smoke plume was sighted, the C-130 crossed the plume centerline at a downwind location and then turned into the wind, following the smoke toward its source. C-130 aircraft sampling time periods and altitudes are shown in Table 2. Background concentrations were measured immediately before and after sampling of the plume (generally ∼30 s to 2.5 min). Differing sampling time delays were accounted for to synchronize all data shown herein. Latitude, longitude, and altitude were sampled at 10 Hz by GPS and averaged to 1 Hz.

Carbon monoxide (CO) was measured at 1 Hz using a vacuum ultraviolet resonance fluorescence instrument (Aero-Laser AL5002). Ozone (O_3) was measured at 1 Hz using an "inverse" NO chemiluminescence instrument. Relative humidity was measured using a Buck Research multistage hygrometer (±5 % uncertainty). An Ultra High Sensitivity Aerosol Spectrometer (UHSAS, Particle Metrics Inc., Boulder, CO) provided size-resolved aerosol number concentrations (0.1–1.0 μm in diameter). Calibration of the UHSAS was performed using standard polystyrene latex spheres, which may underestimate the size of smoke particles, which have lower refractive indices (Reid et al., 2005a); spherical particles were assumed to obtain size-resolved volume distributions, consistent with previous wildfire studies (e.g., Yokelson et al., 2009). Total condensation nuclei (CN) concentrations were measured using a condensation particle counter (CPC, TSI Model 3760),

Table 1. Prescribed burn and ground conditions, provided by the Wyoming BLM, for the RF01 and RF03 smoke plumes.

	RF01 Plume	RF03 Plume
Date	7 November 2007	16 November 2007
Latitude	41°38′06″ N	42°31′04″ N
Longitude	107°23′10″ W	106°21′59″ W
Elevation	2499–2560 m	2267–2359 m
Burn Time	20:00–00:00 UTC	18:45–22:15 UTC
Ambient Temperature	10 °C	8–13 °C
Relative Humidity	26 %	29–36 %
Wind Speed	7–8 m s^{-1}, gusts to 12 m s^{-1}	3–6 m s^{-1}, gusts to 8 m s^{-1}
Burn Area	0.8–0.9 km^2	0.3 km^2
Fuel Type (s)	∼90 % mountain big sagebrush (live), ∼10 % aspen (live)	∼75 % mountain big sagebrush (live), ∼20 % mountain mahogany (dormant), ∼5 % Rocky Mountain juniper
Live Fuel Moisture	∼82 %	∼70 %

Table 2. C-130 aircraft sampling time periods and altitudes for the RF01 and RF03 smoke plumes, as well as the estimated aerosol age, based on C-130 location and wind speed data. For carbon monoxide (CO), ozone (O$_3$), total condensation nuclei (CN), particles >0.1 µm (N$_{>0.1}$), and particles >0.5 µm (N$_{>0.5}$), average background concentrations (with standard deviations in parentheses) are shown along with the range of concentrations observed in the plume. Average horizontal and vertical wind speed, ambient temperature, and relative humidity, measured aboard the C-130 aircraft are shown with standard deviations.

	RF01 Plume	RF03 Plume
Plume Sampling Time Period	21:46:17–21:50:10 UTC	22:08:24–22:26:35 UTC
Aircraft Altitude (AGL)	1034–1807 m	183–3451 m
Sampled Aerosol Age	∼17–30 min	∼ 2 min–∼2 h
Average Background [CO]	81 (1) ppbv	92.6 (0.9) ppbv
Plume [CO]	80–184 ppbv	87–311 ppbv
Average Background [O$_3$]	112 (4) ppbv	102 (4) ppbv
Average Plume [O$_3$]	112 (4) ppbv	93 (7) ppbv
Average Background [CN]	211 (12) cm^{-3}	865 (570) cm^{-3}
Plume [CN]	193–9591 cm^{-3}	203–66061 cm^{-3}
Average Background [N$_{>0.1}$]	56 (19) cm^{-3}	183 (55) cm^{-3}
Plume [N$_{>0.1}$]	33–4949 cm^{-3}	17–12 698 cm^{-3}
Average Background [N$_{>0.5}$]	0.3 (0.9) cm^{-3}	3 (3) cm^{-3}
Plume [N$_{>0.5}$]	0–15 cm^{-3}	0–215 cm^{-3}
Wind Speed, Horizontal	15 (1) m s^{-1}	17 (2) m s^{-1}
Wind Speed, Vertical	0.1 (1.1) m s^{-1}	−0.3 (1.0) m s^{-1}
Ambient Temperature	0.2 (1.5) °C	1.1 (4.2) °C
Relative Humidity	21 (6) %	46 (4) %

detecting particles >∼13 nm in diameter and corrected for coincidence. Aerosol chemical composition was measured using several real-time techniques, described below.

2.2 Aircraft aerosol time-of-flight mass spectrometer (A-ATOFMS)

In-situ measurements of the size-resolved chemical composition of individual submicron particles were made using the recently developed aircraft aerosol time-of-flight mass spectrometer (A-ATOFMS) (Pratt et al., 2009). The A-ATOFMS measures, in real-time, the vacuum aerodynamic diameter

(d_{va}) and dual-polarity mass spectra of individual particles from ∼70–1200 nm (d_{va}). Following a ^{210}Po neutralizer and pressure-controlled inlet (Bahreini et al., 2008), particles are focused in an aerodynamic lens system. Particles are optically detected by two continuous wave 532 nm lasers spaced 6.0 cm apart, providing particle velocity and, thus, d_{va}. Polystyrene latex spheres of known physical diameter from 95–1500 nm were used for the particle size calibration. During ICE-L, particles were desorbed and ionized using 266 nm radiation from a Q-switched Nd:YAG laser operating at ∼0.4–0.6 mJ. Positive and negative ions

resulting from individual particles are detected within the time-of-flight mass spectrometer. For the analysis discussed herein, 162 and 1212 individual particles were chemically analyzed during RF01 and RF03 plume sampling, respectively. Standard errors of particle type number percentages were calculated assuming Poisson statistics. Mass spectral peak identifications correspond to the most probable ions for a given m/z ratio based on previous lab and field studies; the peak area of a specific m/z is related the amount of a specific species on each particle (Bhave et al., 2002).

2.3 Compact time-of-flight aerosol mass spectrometer (C-ToF-AMS)

The Aerodyne compact time-of-flight aerosol mass spectrometer (C-ToF-AMS) ()(Drewnick et al., 2005) measured the mass concentrations of non-refractory species (organics, sulfate, nitrate, ammonium, and a fraction of chloride) in real-time. Particles of d_{va} ∼50–800 nm are focused by an aerodynamic lens system, sent through a 3.5 % chopper, and then impacted onto a tungsten vaporizer operated at 550–560 °C. The chopper can be operated in three modes to gather either background mass spectra, ensemble average mass spectra over all particle sizes, or size-resolved mass spectra. Measurements of chloride and other semi-refractory species are reported herein, but concentrations of these species are significantly underestimated by the C-ToF-AMS because they are not efficiently volatilized at the vaporizer temperature (550–560 °C) used. Once vaporized, molecules undergo electron impact ionization and are extracted at a rate of ∼53 kHz into a time-of-flight mass analyzer. For this airborne deployment, the C-ToF-AMS was fitted with a pressure-controlled inlet (Bahreini et al., 2008) to prevent fluctuations in particle sizing and focusing with ambient pressure.

Detection limits were calculated as the standard deviation of the noise when measuring filtered air (15 s averaging): organics (0.08 µg m^{-3}), sulfate (0.02 µg m^{-3}), nitrate (0.01 µg m^{-3}), ammonium (0.07 µg m^{-3}), and chloride (0.01 µg m^{-3}). In practice, detection is often limited by counting statistics at low aerosol loadings. Considering an average smoke particle density of ∼1.2 g cm^{-3} (Reid et al., 2005b), comparison of the C-ToF-AMS size-resolved mass distribution with the UHSAS volume distribution yields an estimated collection efficiency (CE) (Huffman et al., 2005) of ∼0.28–0.55, similar to a previously derived CE of 0.34 for ambient biomass burning measurements (Capes et al., 2008). Changes in the estimated CE through the plumes suggests changes in particle phase (Matthew et al., 2008), density, and/or the fraction of refractory material; herein, a CE of 0.4 is utilized with reported uncertainties reflecting variability in CE, as well as the mass measurement. In addition, due to possible interference from the abundance of organics (and because nitrate mass loadings were very low), reported nitrate mass concentrations may be a factor of 2–3 high; this

is reflected in the reported uncertainty for the nitrate and organic mass concentrations. Oxygen/carbon (O/C) ratios were calculated from unit resolution mass spectra following the estimation method developed, using a high resolution ToF-AMS, by Aiken et al. (2008):

$$O/C = (0.0382 \pm 0.0005)(x) + (0.0794 \pm 0.0070) \qquad (1)$$

where x is the percentage of organic aerosol mass from m/z 44(CO$_2^+$), which was corrected based on background gas-phase CO$_2$ concentration. Given that CO$_2$ concentrations are enhanced within smoke plumes, this may lead to an overestimation of the organic aerosol mass and O/C ratio.

2.4 Single particle soot photometer (SP2)

Particles containing black carbon (BC) were measured by a single particle soot photometer (SP2, Droplet Measurement Technologies, Boulder, CO), a laser-induced incandescence instrument (Schwarz et al., 2006; Baumgardner et al., 2008). During ICE-L, the SP2 measured BC mass in the range of 0.5–10.5 fg-BC (0.08–0.22 µm BC mass equivalent diameter); BC particles greater than ∼10.5 fg saturate the incandescence detector. Due to the limited BC mass range, scaling factors for the below- and above-detection limit BC masses were generated and applied to estimate total BC mass. The estimated uncertainty in BC mass is ±20 % (Baumgardner et al., 2007); however, variations in BC mass were observed to be greater and thus are noted as the variability in BC mass fraction. The separation between the scattering and incandescent peaks, termed the incandescent lag, was utilized to examine the BC coating thickness where "thinly-coated" BC particles have short incandescent lags (<2 µs) and "thickly-coated" BC particles have longer incandescent lags (>2 µs) (Moteki and Kondo, 2007; Moteki et al., 2007; Subramanian et al., 2010). Since the lower limit of the scattering detector is ∼200 nm, the reported number fraction of thickly-coated BC particles is likely a lower limit (Subramanian et al., 2010).

2.5 Cloud activation measurements

CCN number concentration measurements were made using a stream-wise thermal gradient CCN counter (Droplet Measurement Technologies, Boulder, CO), described previously in detail by Roberts and Nenes (2005). During plume measurements, water supersaturation was held constant at 0.5 %. CCN concentrations were corrected for ambient temperature and pressure. The number concentrations of ice-nucleating aerosol particles were measured in real-time using a continuous flow diffusion chamber (CFDC) (Rogers et al., 2001; Eidhammer et al., 2010). By simulating cloud conditions at relative humidities exceeding 102 % (with respect to water), the CFDC emphasized condensation/immersion freezing nucleation. Use of an impactor limited sampling to primarily submicron particles (<∼1.5 µm in aerodynamic diameter) prior

to CFDC processing in order to distinguish ice crystals nucleated in the CFDC from non-activated aerosol particles using optical methods.

3 Results and Discussion

3.1 Prescribed burn and plume conditions

In November 2007, two Wyoming BLM prescribed burn smoke plumes were characterized by instruments on the NSF/NCAR C-130 aircraft. Ground-based details of the burns are noted in Table 1. The fuels of the RF01 and RF03 burns were dominated by live mountain big sagebrush (*Artemisia tridentate* ssp. *vaseyana*) ($\sim$90 % and $\sim$75 %, respectively) with fuel moistures estimated at $\sim$82 % and $\sim$70 %, respectively. From ground-based observations, the RF01 burn was characterized as a flaming fire with 3–5 m flame lengths and a burn rate of 0.8–1.0 km h^{-1}. Although the RF03 burn was also characterized as a flaming fire, a smoldering component was observed to be associated with the dormant mountain mahogany *(Cercocarpus)*. These prescribed burns were relatively small with burn areas of $\sim$0.8–0.9 km^2 and 0.3 km^2, respectively, too small for detection by satellite imagery. Photographs of the RF03 prescribed burn location prior to the burn, as well as the smoke plume as viewed from the C-130 aircraft, are shown in Fig. 1.

3.1.1 Smoke plume RF01

The C-130 aircraft intersected the RF01 smoke plume for a period of $\sim$4 min (aircraft time) with sampling occurring at 1.0–1.8 km above ground level, as shown in Table 2. Based on average wind speeds, burn location, and flight path, the transport time of the smoke plume particles sampled was $\sim$17–30 min from the burn source to the sampling points. CO concentrations within the plume (80–184 ppbv) were up to 2.3 times greater than those measured in the nearby background air (81$\pm$1 ppbv). O$_3$ concentrations within the plume were similar to background conditions; however, longer plume aging may be required for the photochemical production of O$_3$ (Goode et al., 2000; Yokelson et al., 2009). Total CN number concentrations within the smoke plume (193–9591 cm^{-3}) were up to $\sim$45 times greater than background conditions (211$\pm$12 cm^{-3}). Similarly, number concentrations of particles with 0.11-0.1 µm diameters ($N_{>0.1}$) (33–4949 cm^{-3}) were elevated by up to a factor of $\sim$88 compared to background concentrations (56$\pm$19 cm^{-3}). ΔCN/ΔCO ratios, calculated by dividing excess CN ([CN] – [CN$_{background}$]) by excess CO ([CO] – [CO$_{background}$]), ranged from 2–3261 cm^{-3} ppbv^{-1}. Similarly, $\Delta N_{>0.1}$/ΔCO ratios were 0.6–347 cm^{-3} ppbv^{-1}, which span a larger range and a higher values than previous measurements of fresh Amazonian smoke ($<$76 cm^{-3} ppb^{-1}) summarized by Guyon et al. (2005). For this small section of the plume,
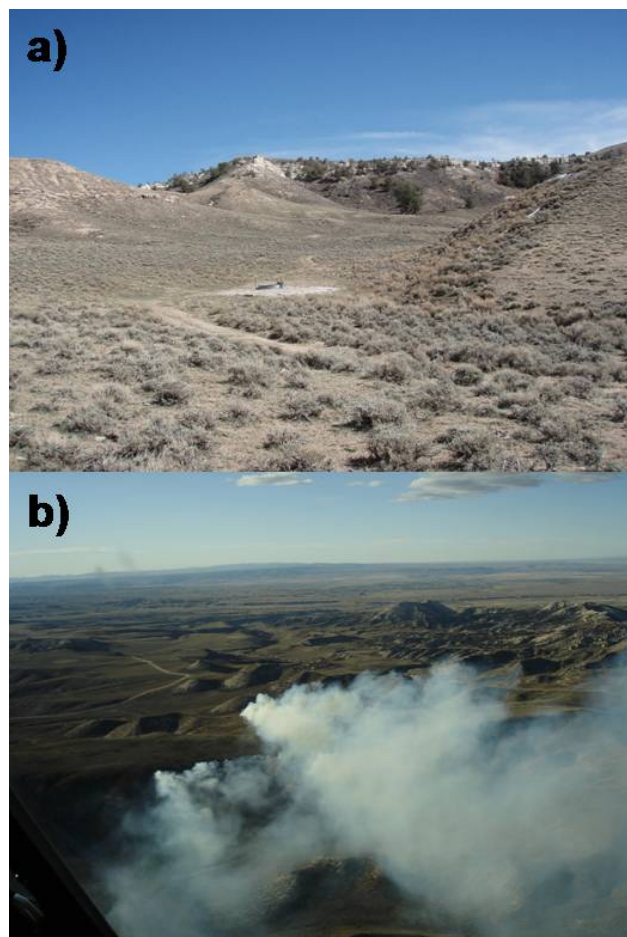
Fig. 1. Photographs of the RF03 prescribed burn: **(a)** location prior to the burn (courtesy of Kristi Bulock) and **(b)** smoke plume as viewed from the C-130 aircraft (courtesy of David Rogers).

ΔCN and $\Delta N_{>0.1}$ were not highly correlated with ΔCO ($R^2 = 0.29$ and 0.38, respectively).

3.1.2 Smoke plume RF03

The RF03 smoke plume was sampled for $\sim$18 min (aircraft time) at 0.2–3.5 km above ground level, as described in Table 2. Four time periods were selected to focus analyses during this long time interval. Period 1 corresponds to the sampling closest to the burn, where smoke particle age was calculated to be $\sim$2–4 min. The furthest sampling point from the burn source corresponded to a smoke age of $\sim$117 min. This long span allows an examination of transformations as the smoke particles aged.

The temporal profile of size-resolved particle number concentrations with associated CO and O$_3$ concentrations is shown in Fig. 2. Large variations in the measurements reflect the meandering of this small plume and the effects of turbulence mixing with the relatively clean background. Since CO data are not available for sampling closest to the burn source,

Table 3. Submicron aerosol mass fractions, shown as percentages with uncertainty ranges, considering black carbon, measured by the SP2, as well as non-refractory organics, sulfate, nitrate, ammonium, and chloride, measured by the C-ToF-AMS for the four RF03 plume periods, as well as the RF01 plume average. Data are illustrated in Fig. 3.

	RF03 Age				RF01 Average
	~2–4 min	~32–39 min	~52–62 min	~81–88 min	~17–30 min
Black carbon (SP2)	5 [0.3–13]	13 [9–17]	20 [6–34]	11 [–16]	2 [0.04–6]
Organics	89 [80–98]	71 [55–94]	66 [23–100]	61 [32–98]	86 [28–100]
Nitrate	3 [1–3]	8 [2–10]	8 [1–12]	7 [1–12]	5 [1–9]
Sulfate	0.6 [0–1]	4 [3–5]	4 [2–6]	17 [8–27]	4 [2–6]
Ammonium	0.3 [0.2-0.4]	2 [1–4]	2 [0–5]	3 [0–13]	2 [0.1–3]
Chloride	2 [0.8–2]	1 [0.8–2]	0.9 [0.1–2]	0.4 [0–2]	0.9 [0.2–2]
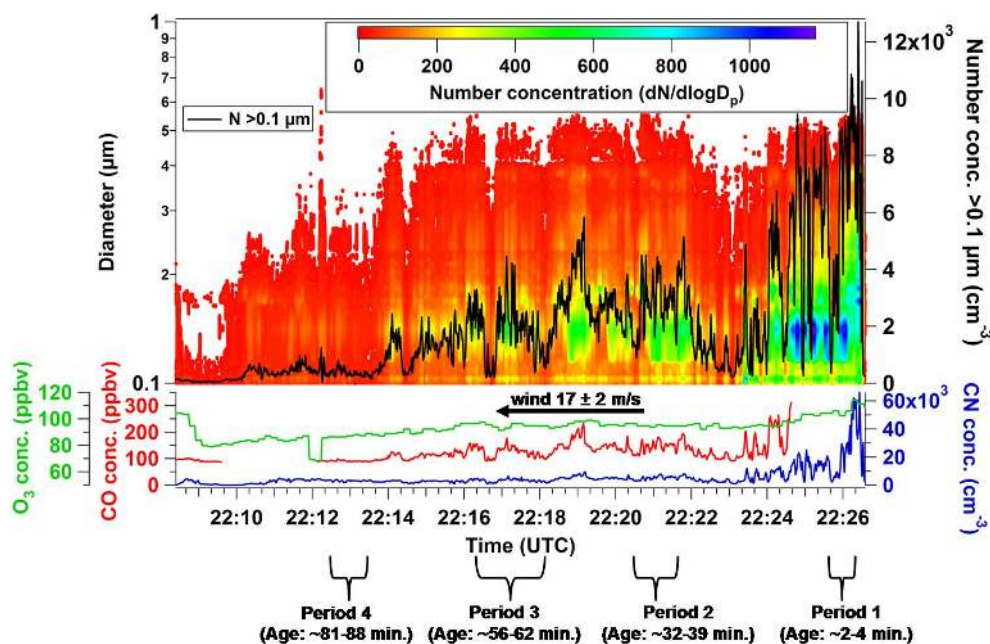
Fig. 2. RF03 temporal profiles of UHSAS size-resolved particle number concentrations are illustrated with associated concentrations of CO, O_3, CN, and particles $>0.1\,\mu m$. Since CO data are not available for sampling closest to the burn source, maximum concentrations are estimated to be greater than the highest measured value of 311 ppbv, well above the average background air concentration of 92.6 ± 0.9 ppbv. The aircraft was flying into the wind, as indicated by the arrow; therefore, later sampling times correspond to sampling closer to the fire source. Discussed time periods and calculated smoke plume ages are noted.

maximum concentrations are estimated to be greater than the highest measured value of 311 ppbv, well above the background air concentration of 92.6 ± 0.9 ppbv. Consistent with sampling closer to the burn source, CN number concentrations (203–$66061\,cm^{-3}$) were up to ~76 times greater than background conditions near the fire source ($865\pm570\,cm^{-3}$). Similarly, $N_{>0.1}$ number concentrations (17–$12698\,cm^{-3}$) were elevated by up to a factor of ~70 compared to background concentrations ($183\pm55\,cm^{-3}$). As shown in Fig. 2, the particle diameter mode of the fresh smoke particles was ~170 nm, consistent with previously reported count median diameters of 100-160 nm for fresh smoke (Reid et al., 2005b). Although CO concentrations are not available for

the entire plume, $\Delta x/\Delta CO$ ratios were calculated for the remainder of the plume (see Fig. 2 for measurement periods). $\Delta CN/\Delta CO$ ratios ranged from 3–$11\,520\,cm^{-3}\,ppbv^{-1}$; similar to RF01 plume sampling, a high correlation between ΔCN and ΔCO was not observed ($R^2 = 0.30$). However, a high correlation was observed between $\Delta N_{>0.1}$ and ΔCO ($R^2 = 0.93$). O_3 concentrations peaked at 114 ppbv near the RF03 plume source, steadily decreased below even background conditions to 79 ppbv within the plume, and rose back to 103 ppbv with mixing with background air (prior to 22:09:14) (Fig. 2), suggesting initial O_3 production, followed by O_3 destruction within the plume. This contrasts the reported photochemical production of O_3 in the presence of

NO_x observed within most biomass burning plumes during aging (e.g. Goode et al., 2000; Hobbs et al., 2003); however, periods of negative ΔO_3 have been observed for smoke ages <5 min (Hobbs et al., 2003) and low ultraviolet intensities (Stith et al., 1981). The production or loss of O_3 is dependent on NO_x concentrations, wherein HO_2 radicals formed from the oxidation of CO can react with O_3 to form OH rather than reacting with NO (Crutzen et al., 1999). In this study, the observed O_3 destruction following an initial possible burst of O_3 production is difficult to interpret without the measurement of other gas phase species, particularly NO_x.

The next sections describe the evolution of particle chemistry, as a function of particle age from the source of the burn. The fresh samples (~2–4 min in age) are described first, followed by the more aged samples.

3.2 Fresh biomass burning chemical signature

The chemical composition of smoke plume particles was measured within the RF03 smoke plume from 22:25:57–22:26:31 UTC (Period 1), corresponding to a plume age of ~2–4 min. Overall, the fresh biomass burning particles were observed, by C-ToF-AMS, SP2, and A-ATOFMS, to be internal mixtures of organic carbon, elemental carbon, and potassium chloride and sulfate salts. Mass concentrations of submicron non-refractory species, including organic carbon, nitrate, sulfate, ammonium, and a fraction of chloride, were measured by the C-ToF-AMS; black carbon mass concentrations were measured by the SP2. The mixing of individual chemical species within single particles was measured by A-ATOFMS. Based on C-ToF-AMS and SP2 measurements, the average mass fractions [with uncertainty ranges] for these fresh (Period 1) smoke plume particles were estimated to be 89 % [80–98 %] organics, 5 % [0.3–13 %] black carbon (BC), 3 % [1–3 %] nitrate, 0.6 % [0–1 %] sulfate, 0.3 % [0.2–0.4 %] ammonium, and 2 % [0.8–2 %] chloride (Table 3 and Fig. 3). These results are in good agreement with previous measurements of fresh dry smoke particle composition: ~80 % OC, ~5–9 % BC, and ~12–15 % trace inorganics, such as potassium, sulfate, chloride, and nitrate (Reid et al., 2005b). It is important to note that traditional filter-based BC measurements can overestimate BC mass due to interferences from organics (Subramanian et al., 2007; Subramanian et al., 2010). The mass fractions calculated herein assume that refractory species not measured by the C-ToF-AMS and SP2 contribute only minor fractions to the total submicron mass, providing upper limits for the species mass fractions. Refractory species, such as potassium salts and mineral dust, are not measured by the C-ToF-AMS, which operated with a vaporizer temperature of 550–560 °C. Volatilization rates of KCl and K_2SO_4 become important at 700–800 °C and above 1000 °C, respectively (Knudsen et al., 2004). Previous measurements of burning dry sagebrush have shown contributions of potassium and chloride up to ~24 % and ~10 % of the total
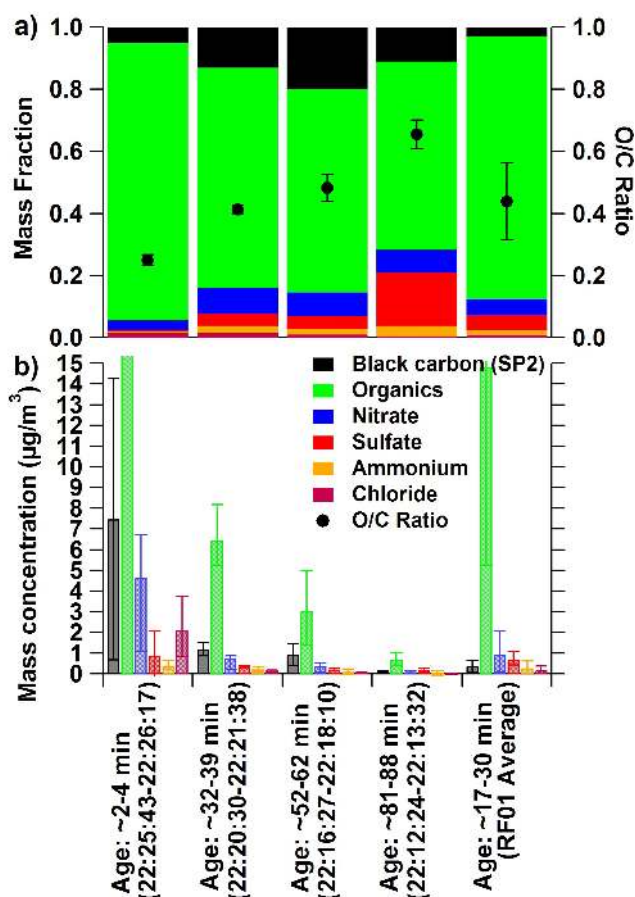
Fig. 3. (a) Submicron aerosol mass fractions considering black carbon, measured by the SP2, as well as non-refractory organics, sulfate, nitrate, ammonium, and chloride, measured by the C-ToF-AMS for the four RF03 plume periods, as well as the RF01 plume average. Uncertainty ranges in the mass fractions are noted in Table 3. The O/C ratio of the organics, measured by the C-ToF-AMS, is also illustrated. **(b)** Submicron average species mass concentrations measured by the SP2 and C-ToF-AMS; note that average organic mass concentrations during Period 1 (age ~2–4 min) and RF01 are offscale: 129 [88–195] $\mu g\,m^{-3}$ and 15 [5–33] $\mu g\,m^{-3}$, respectively.

aerosol mass, respectively, which were significantly higher than other tested fuels (Chen et al., 2007). The presence of these species within the fresh biomass burning particles was confirmed by A-ATOFMS. In addition, refractory OC, shown previously to contribute to biomass burning aerosols (Clarke et al., 2007), may not be measured by the C-ToF-AMS.

Throughout RF03 plume sampling, 84±1 % of the submicron (~0.1–1.0 μm) particles by number were identified by A-ATOFMS as having one dominant biomass burning mass spectral signature, characterized by potassium internally mixed with carbonaceous species (Silva et al., 1999; Hudson et al., 2004). The average positive and negative ion mass spectra of the fresh (Period 1) biomass burning
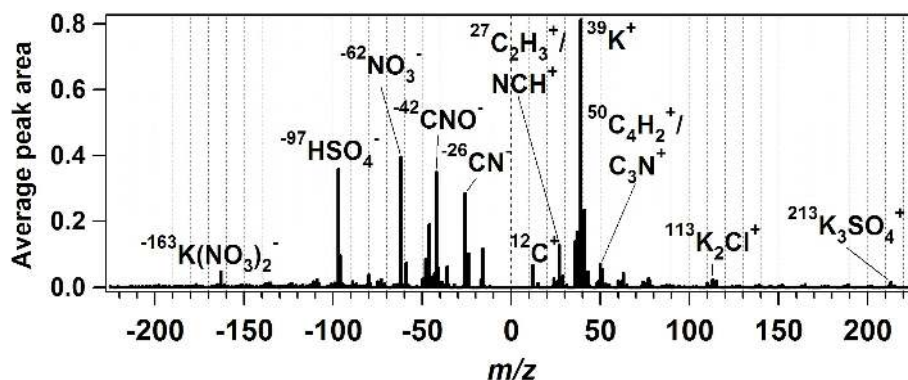
**Fig. 4.** A-ATOFMS average mass spectrum of 52 fresh biomass burning particles sampled during RF03 plume Period 1.

particles are shown in Fig. 4. The particles were characterized by potassium (m/z 39/41(K^+), 78(K_2^+)), organic carbon (OC) and organic nitrogen (m/z 27($C_2H_3^+$/NCH$^+$), 37(C_3H^+), 50($C_4H_2^+$/C_3N^+), -26(CN$^-$), -42(CNO$^-$)), elemental carbon (EC) ($C_n^{+/-}$), nitrate (m/z -46(NO$_2^-$), -62(NO$_3^-$)), and sulfate (m/z -80(SO$_3^-$), -97(HSO$_4^-$)), similar to observations by Silva et al. (1999) in laboratory studies. Potassium sulfate (m/z 213($K_3SO_4^+$)), potassium nitrate (m/z -163(K(NO$_3$)$_2^-$)), and potassium chloride (m/z 113/115(K_2Cl^+), -109/-111(KCl$_2^-$)) were also present in ∼63–73 % of the fresh biomass burning particles, likely due to the contribution from flaming combustion (see Sect. 3.1), as potassium concentrations have been observed to decrease exponentially from flaming to smoldering combustion (Cahill et al., 2008). While previous studies have shown primarily KCl in fresh biomass burning aerosols with little contribution from sulfur species (Li et al., 2003), the presence of K_2SO_4 has been suggested to be a function of fuel composition and burn conditions (Pósfai et al., 2003). Consistent with the very low mass fraction of ammonium observed by the C-ToF-AMS, only 8±4 % of the fresh biomass burning particles were observed by A-ATOFMS to be internally mixed with ammonium (m/z 18 (NH$_4^+$)). Despite the low mass fractions of nitrate and sulfate observed by the C-ToF-AMS during Period 1, 100 % of these fresh (Period 1) biomass burning particles by number were internally mixed with nitrate (m/z -62(NO$_3^-$)) and 92±4 % contained sulfate (m/z -97(HSO$_4^-$)), as measured by A-ATOFMS. This is a significant finding, showing that all freshly-emitted biomass burning particles contain some hygroscopic material at the point of emission, even if initially at low mass concentrations. This has important ramifications for cloud formation in regions of major fires.

The C-ToF-AMS size distribution of organics during RF03 Period 1 shows the mass diameter peaking at ∼270 nm d_{va}. The organics were characterized by an O/C ratio of 0.25±0.02, which is in excellent agreement with fresh laboratory biomass burning organics (O/C ratio 0.15 to 0.39)

(Weimer et al., 2008; Grieshop et al., 2009). An ion peak at m/z 60, attributed to levoglucosan (Schneider et al., 2006; Alfarra et al., 2007), a degradation product of cellulose (Simoneit et al., 1999), comprised 1.09 ±0.04 % of the total organic signal, in agreement with previous AMS observations of 1–7 % (Weimer et al., 2008; Grieshop et al., 2009). Further, laboratory measurements of levoglucosan/OC mass ratios for PM$_{2.5}$ resulting from sage combustion were previously observed to be 1.6–4.1 % (Sullivan et al., 2008). In agreement, A-ATOFMS measurements suggested that 40±7 % of the fresh biomass burning particles contained levoglucosan (m/z -71(C$_3$H$_3$O$_2^-$)) and 60±7 % contained oxalate (m/z -89(C$_2$O$_4$H$^-$)) (Sullivan and Prather, 2007), consistent with previous filter-based observations of Gao et al. (2003).

Consistent with the results discussed herein, previous single-particle mass spectrometry observations of a ∼2 h old large forest fire plume showed over 90 % of the particles contained potassium, being classified as having a biomass burning mass spectral signature (Hudson et al., 2004). Similarly, using electron microscopy, organic particles with crystalline potassium salt inclusions were observed to be the most abundant type in smoke plumes (Pósfai et al., 2003). Within the sampled RF01 and RF03 smoke plumes, 33±4 % and 16±1 %, respectively, of the submicron particles were not classified by the biomass burning mass spectral signature. All EC was observed by the A-ATOFMS to be internally mixed with OC, in agreement with the Hudson et al. (2004) study. Any EC particles smaller than 70 nm (d_{va}), not examined in this study, would comprise a minor fraction of the particle number and mass fractions, given the size mode at ∼170 nm (Fig. 2). This A-ATOFMS observation of EC internally mixed within the biomass burning particles is consistent with the RF03 SP2 measurements, which showed that ∼47 % of the measured BC (defined here as EC + polycyclic aromatic hydrocarbons) particles (0.08–0.22 µm BC mass equivalent diameter) were thickly-coated during Period 1 (aerosol age ∼2–4 min). This is consistent with the smoldering component of the RF03 prescribed burn.
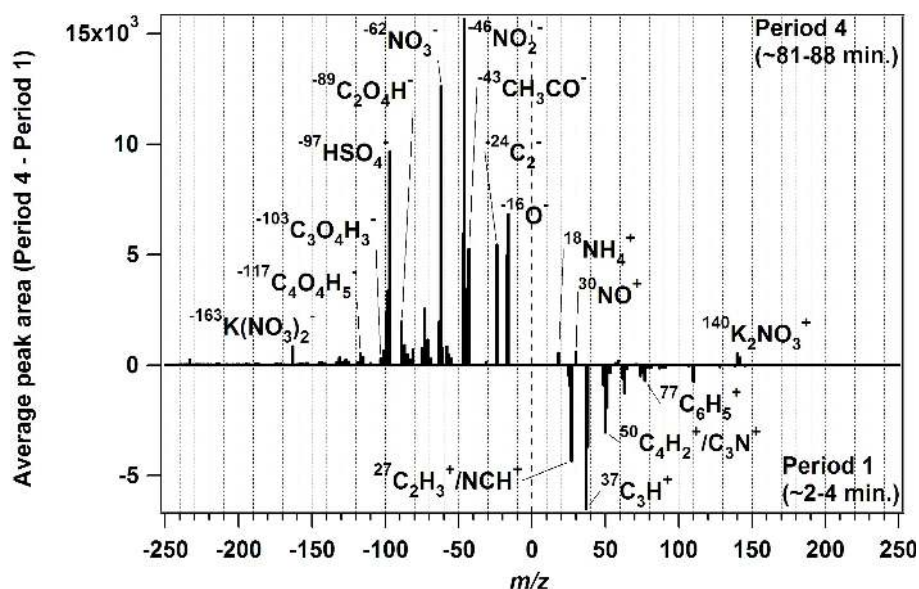
Fig. 5. A-ATOFMS average positive and negative ion mass spectra for biomass burning particles during RF03 Period 1 (age ~2–4 min) subtracted from biomass burning particles during RF03 Period 4 (age ~81–88 min). Positive intensity ion peaks indicate species added during aging of the individual biomass burning particles; negative intensity ion peaks indicate species with higher ion intensities within the fresh particles. Only ion peaks above 95 % confidence limits following subtraction are shown.

For the RF03 plume, an average of 2 % of the submicron particles by number were classified by the A-ATOFMS as OC internally mixed with sulfate and nitrate; a larger fraction (28±4 %) of these OC particles were observed within the RF01 plume. For the RF03 and RF01 plumes, 0.7±0.2 % and 2±1 %, respectively, of the particles were classified as EC mixed with OC, sulfate, and nitrate. Mineral dust, which is lofted from the ground during fires, contributed 1.4±0.3 % and 2±1 %, respectively to the RF01 and RF03 plume submicron particles by number. This is consistent with the minor contributions observed previously by Li et al. (2003). Finally, 11±1 % and 2±1 % of the particles in the RF01 and RF03 plumes, respectively, produced only negative ion mass spectra containing nitrate and sulfate; the origin of these particles is still being investigated. They could be representative of particles with thicker nitrate coatings due to gas-to-particle condensation occurring at cooler temperatures.
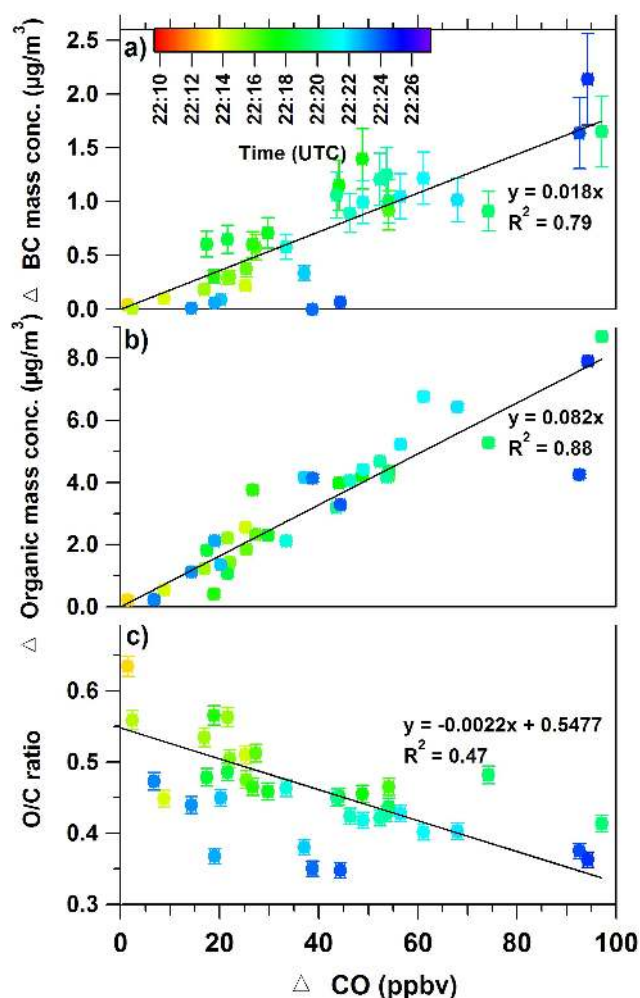
3.3 Aging of smoke plume particles

RF03 plume sampling corresponded to particles ranging from ~2 min to ~2 h in age; whereas, the single, shorter RF01 plume sampling period corresponded to ~17–30 min aged particles (Table 2). Thus, aging of the RF03 plume particles across the plume is discussed herein and compared to the RF01 plume average. A comparison of the A-ATOFMS average mass spectral signatures for the RF03 Period 1 and Period 4 biomass burning particles is shown in Fig. 5. As expected, excess black carbon mass concentrations ($\Delta BC = [BC] - [BC_{background}]$), measured by the SP2, were

linearly correlated with ΔCO ($R^2 = 0.79$, Fig. 6a) through the RF03 smoke plume, showing that BC mass concentration changes were consistent with dilution. Average $\Delta BC/\Delta CO$ was observed to be $0.018\pm0.001\,\mu g\,m^{-3}\,ppbv^{-1}$, slightly higher than previously observed by Hobbs et al. (2003) for a savanna fire ($0.0056–0.0105\,\mu g\,m^{-3}\,ppbv^{-1}$) using a filter-based optical transmission technique to measure BC. BC mass fractions were similar (within uncertainties) for all time periods, including the RF01 plume (Table 3).

3.3.1 Organics

Excess organic mass concentrations (above background conditions), measured by the C-ToF-AMS, were linearly correlated with ΔCO ($R^2 = 0.95$, Fig. 6b) for the RF03 plume. However, a straightforward dilution did not occur as the organic aerosol composition changed within the plume with the O/C ratio increasing with decreasing ΔCO (Fig. 6c), similar to the observations of Capes et al. (2008). Over the course of RF03 plume sampling, the O/C ratio increased from 0.25±0.02 for an aerosol age of ~2–4 min to 0.65±0.05 for an aerosol age of ~81–88 min (Fig. 3a). The intermediate O/C ratio of 0.44±0.12 measured for the RF01 plume (aerosol age ~17–30 min) is consistent with the oxidation timescale observed for the RF03 plume (Fig. 3a). The increasing O/C ratio with aging is consistent with an increasingly oxygenated organic aerosol (Aiken et al., 2008; Heald et al., 2010). Hawkins and Russell (2010) observed the formation of carboxylic acid groups with loss of ketone groups, significantly increasing the O/C ratio, in the aging of biomass

Fig. 6. Excess (Δ) **(a)** SP2 black carbon (BC) mass concentrations and **(b)** C-ToF-AMS organic mass concentrations versus ΔCO concentrations as a function of RF03 plume sample time. **(c)** C-ToF-AMS organic O/C ratio versus ΔCO as a function of RF03 plume sample time. Note that CO data were not available over the entire RF03 smoke plume (see Fig. 2).

the gas phase following heterogeneous reactions and/or dilution, resulting in a more oxidized organic aerosol (Kroll et al., 2009), as well as (2) condensation of oxidized organics (Donahue et al., 2006), such as dicarboxylic acids, as discussed below. As noted by Capes et al. (2008) and Hennigan et al. (2011) for similar observations of the aging of biomass burning organic aerosol, the mechanisms must balance one another to keep the Δorganic/ΔCO ratio constant.

Consistent with the increased fraction of oxidized organics measured by C-ToF-AMS, A-ATOFMS measurements of biomass burning particles show increased ion peaks areas, proportional to mass, associated with oxidized organics (m/z 43(CH_3CO^+)), and decreased ion peak areas for non-oxygenated organics (e.g. m/z 27($C_2H_3^+$), 37(C_3H^+), 50($C_4H_2^+$), 77($C_6H_5^+$)) with aging, as shown in Fig. 5. Further, the C-ToF-AMS O/C ratio was correlated ($R^2 = 0.5$) with the A-ATOFMS oxidized organics/total organics ratio, calculated by dividing the relative peak area of m/z 43(CH_3CO^+) by the sum of the relative peak areas of representative organic ions (m/z 27($C_2H_3^+$), 29($C_2H_5^+$), 37(C_3H^+), 43(CH_3CO^+)), as defined by Spencer and Prather (2006). A-ATOFMS measurements show the accumulation of organic acids on biomass burning particles as the plumes aged (Fig. 5). In general, organic acids have been shown to account for >3% of particle mass in aged smoke particles compared to <1% in fresh smoke (Reid et al., 2005b). The number fraction of biomass burning particles containing oxalate (m/z -89($C_2O_4H^-$)) increased from 60 ± 7% to 94 ± 4% with aging from ~2–4 min to ~81-88 min within the RF03 plume, with the RF01 plume showing an intermediate fraction (87 ± 3%), as expected. Concurrent with the increased fraction of particles internally mixed with oxalate, the average m/z -89 peak area, which is proportional to oxalate mass, also increased by a factor of 6 ± 4, as illustrated in Fig. 5. Similarly, the number fractions of biomass burning particles internally mixed with malonate (m/z -103($C_3O_4H_3^-$)) and succinate (m/z -117($C_4O_4H_5^-$)) (Sullivan and Prather, 2007) also increased significantly from 15 ± 5% and 25 ± 6%, respectively, to 66 ± 8% and 77 ± 7%, respectively, with aging from ~2–4 min to ~81–88 min within the RF03 plume, with the RF01 plume showing an intermediate fraction. Similar to oxalate, the A-ATOFMS malonate and succinate peak areas, proportional to mass, increased by factors of 5 ± 4 and 8 ± 5, respectively, with aging, as shown in Fig. 5. These data are consistent with previous smoke plume observations of the concentrations of oxalate and succinate increasing by at least an order of magnitude after ~40 min of aging, although malonate was absent from most of the savanna fire aerosols (Gao et al., 2003). Gao et al. (2003) concluded that the most likely pathways for the addition of dicarboxylic acids during biomass aging are the oxidation of larger organic molecules at the particle surface through heterogeneous reactions or aqueous reactions inside the particle. However, Yokelson et al. (2009)

burning organic aerosol; however, the timescale of oxygen uptake via heterogeneous reaction with OH alone is too slow to explain the increased O/C ratios here (DeCarlo et al., 2008; Kessler et al., 2010). Considering the O/C ratio of the nearby background organic aerosol (0.61–0.95), ~25% of the observed bulk O/C ratio increase from RF03 Periods 1–3 is estimated to be due to mixing with background aerosol, using the method of Murphy et al. (2009). For Period 4, this dilution influence increases to over 50%; however, this estimate is highly uncertain given the low loadings of this period and the background, as well as the still high abundance of biomass burning particles, measured by A-ATOFMS. Since the Δorganic/ΔCO ratio was relatively constant, it is likely the aerosol transformed by: (1) repartitioning of more volatile, less oxygenated organic species to

observed formation of gas-phase organic acids within aging smoke plumes. Thus, additional laboratory studies under relevant ambient conditions are required to further understand the mechanism(s) of plume aging resulting in a more oxidized organic aerosol. These studies should strive to reproduce relevant oxidant and precursor concentrations, as well as dilution conditions and temperatures.

Levoglucosan, a degradation product of cellulose, is often used as a marker of fresh biomass burning (Simoneit et al., 1999). ∼40–65 % of the biomass burning particles, by number measured by the A-ATOFMS, were characterized by m/z -71 ($C_3H_3O_2^-$), previously observed to be a marker of levoglucosan (Silva et al., 1999). The contribution of the C-ToF-AMS marker of levoglucosan, m/z 60, to the total organic aerosol decreased from 1.09±0.04 % to 0.3±0.5 % with aging from ∼2–4 min to ∼81–88 mins within the RF03 plume. However, for the RF01 plume average (age ∼17–30 min), the m/z 60 fraction was higher at 1.3±0.1 %. While atmospheric lifetimes of levoglucosan have been estimated at ∼0.7–11 days (Hennigan et al., 2010; Kessler et al., 2010), recently Hennigan et al. (2011) observed a rapid decay, five times faster than the OH collision rate, of levoglucosan in the photooxidation of open biomass burning emissions.

3.3.2 Chloride

Gao et al. (2003) observed chloride mass concentrations to decrease by a factor of two from ∼7–40 min of aging; however, the possible decreasing trend was unclear due to a lack of data points. In this study, average C-ToF-AMS non-refractory chloride mass fractions were within standard deviations for all plume periods (Table 3). Electron microscopy studies have noted the transformation of KCl to K_2SO_4 and KNO_3 during aging (Li et al., 2003; Yokelson et al., 2009). Similarly, the A-ATOFMS number fraction of biomass burning particles with the potassium chloride ion peak m/z 113(K_2Cl^+) decreased slightly with plume aging from 67±7 % to 46±8 % with aging from ∼2–4 min to ∼81–88 min within the RF03 plume; however, average m/z 113(K_2Cl^+) and m/z -35(Cl^-) peak areas, proportional to mass, were within uncertainties for all periods, similar to the C-ToF-AMS data. For the RF01 plume biomass burning particles, 80±4 % by number were characterized by m/z 113(K_2Cl^+), suggesting that the fraction of particles containing potassium chloride salts likely varies for different fuels and fire conditions. In fact, different chloride emission factors were observed by McMeeking et al. (2009) for different fuels, with sagebrush having one of the highest emission factors measured. Indeed, the RF01 fire was characterized by a higher sagebrush fuel fraction (∼90 %) compared to that of the RF03 plume (∼75 %) (Table 1).

3.3.3 Ammonium, nitrate, and sulfate

During smoke plume aging, aerosols accumulate sulfate and nitrate by acquiring NO_x and SO_2 oxidation products (e.g. Gao et al., 2003; Hudson et al., 2004; Yokelson et al., 2009). In particular, several studies have shown the transformation of KCl to K_2SO_4 and KNO_3 during plume aging (Gaudichet et al., 1995; Li et al., 2003; Yokelson et al., 2009). Hobbs et al. (2003) and Gao et al. (2003) observed significant increases in nitrate mass concentrations with plume aging of ∼40 min. During the RF03 smoke plume, excess nitrate and ammonium (plume minus background concentrations), measured by the C-ToF-AMS, were positively correlated ($R^2 = 0.66$), suggesting the addition of ammonium nitrate with aging, confirmed by the A-ATOFMS single-particle mixing (Fig. 5). Initial increases in the mass fractions of ammonium and nitrate were measured from 0.3 % [0.2–0.4 %] and 2 % [1–4 %], respectively, for an aerosol age of ∼2–4 min (Period 1) to 3 % [1–3 %] and 8 % [2–10 %], respectively, for an age of ∼32–39 min (Period 2), after which the mass fractions stayed constant (Table 3 and Fig. 3a). Correspondingly, the number fraction of biomass burning particles, measured by A-ATOFMS, internally mixed with ammonium (m/z 18(NH_4^+)) increased from 8±4 % to 28±4 % from Period 1 to Period 2 with increased ammonium peak areas for the aged particles, as shown in Fig. 5. Nearly 100 % of all biomass burning particles, measured by the A-ATOFMS, were internally mixed with nitrate; nitrate (m/z -62(NO_3^-)) peak area increased by a factor of 3±1 from Period 1 to Period 2 and then stayed constant, consistent with the C-ToF-AMS observations. Similarly, the number fraction of biomass burning particle mass spectra characterized by m/z -125(H(NO_3)$_2^-$) increased from 21±6 % to 59±5 % from Period 1 to Period 2, indicative of increasing nitrate mass on the individual particles. While the number fraction of biomass burning particles internally mixed with potassium nitrate (m/z -163(K(NO_3)$_2^-$)) did not show a clear trend with aging, the ion peak area increased by a factor of 3±2 with aging from RF03 Period 1 (age ∼2–4 min) to Period 4 (age ∼81–88 min).

Liu et al. (2000) noted excess sulfate beyond that required for chloride replacement during smoke plume aging. During RF03 plume aging, the C-ToF-AMS sulfate mass fraction increased from 0.6 % [0-1 %] with ∼2–4 min of aging to 17 % [8–27 %] following ∼81-88 min of aging (Table 3 and Fig. 3a). Accordingly, excess sulfate was not correlated with ΔCO or ammonium. Nearly 100 % of all biomass burning particles were internally mixed with sulfate during all periods, as measured by A-ATOFMS; however, sulfate (m/z -97(HSO_4^-)) peak areas increased by a factor of 3±2 with aging from ∼2–4 min to ∼81–88 min, consistent with the C-ToF-AMS results. Previously, Hudson et al. (2004), using single-particle mass spectrometry, measured higher median sulfate peak areas for aged, or transported, biomass burning events compared to fresh biomass burning particles.

The number fraction of biomass burning particles internally mixed with potassium sulfate (m/z 213($K_3SO_4^+$)) did not show a clear trend with aging.

During RF03 Period 1, the calculated C-ToF-AMS NH_{4meas}^+/NH_{4neu}^+ ratio (Zhang et al., 2007) was calculated to be 0.40±0.08, indicating the presence of acidic particles. The A-ATOFMS number fraction of acidic particles increased with aging, as evidenced by the trend of the sulfuric acid ion marker m/z −195($H_2SO_4HSO_4^-$)) (Denkenberger et al., 2007; Yao et al., 2011). The number fraction of biomass burning particles internally mixed with sulfuric acid increased from 8±4 % at ∼2–4 min of aging to 28±4 % at ∼32–39 min and then stayed relatively constant with aging to ∼81–88 min. For a plume age of ∼17–30 min, 12±3 % of RF01 biomass burning particles were mixed with sulfuric acid.

3.4 Cloud activation properties

3.4.1 Cloud condensation nuclei

Wildfires serve as large sources of CCN (Hobbs and Radke, 1969; Eagan et al., 1974) with a wide range of hygroscopicities (Petters et al., 2009a; Carrico et al., 2010). During RF03 plume aging from ∼2–4 min (Period 1) to ∼81–88 min (Period 4), CCN number concentrations, measured at a supersaturation of 0.5 %, ranged from ∼15 000 cm^{-3} to ∼350 cm^{-3} (Table 4) primarily due to dilution. Background RF03 CCN$_{0.5\%}$ concentrations were ∼230 cm^{-3}. For an assessment of CCN efficiency, the fractions of CCN relative to the $N_{>0.1}$ and total CN (>13 nm) concentrations were calculated. For all periods of plume sampling, CCN$_{0.5\%}$/N$_{>0.1}$ ratios were greater than 1, suggesting activation at 0.5 % supersaturation of all particles greater than 100 nm in diameter throughout the smoke plumes. However, it should be noted that smaller, more hygroscopic particles may have activated before larger, less hygroscopic particles, as observed previously for laboratory smoke particles (Petters et al., 2009a). For the youngest smoke particles (Period 1), the average CCN$_{0.5\%}$/CN ratio was 1.12±0.26, showing that nearly all particles activated at 0.5 % supersaturation (Table 4), as predicted by Petters et al. (2009a) based on laboratory measurements and modeling. Previously, sagebrush smoke particles were observed by Petters et al. (2009a) to be amongst the most hygroscopic of 24 tested biomass fuels. Lower CCN$_{0.5\%}$/CN ratios were observed for RF03 Periods 2 and 3 (∼59 %), as well as for the RF01 plume (∼28 %), despite higher mass fractions of non-refractory sulfate and nitrate measured by the C-ToF-AMS. The lowest CCN$_{0.5\%}$/CN ratio (∼11 %) was measured during Period 4 and is associated with the increased number concentration of <100 nm particles (likely from mixing with background air). It is generally observed that CCN efficiency increases with smoke particle aging (Andreae and Rosenfeld, 2008). Condensation of components with low hygroscopicity still decreases the critical

supersaturation due to the increase in particle size (Petters et al., 2009a); therefore, increased CCN activity with particle aging is expected. Overall, the biomass burning particles were found to be highly CCN active, particularly in contrast to the background aerosol.

3.4.2 Ice nuclei

IN can be produced by biomass combustion events (Hobbs and Locatelli, 1969; Pueschel and Langer, 1973), but the exact source of IN remains unidentified both in the laboratory (Petters et al., 2009b) and in the atmosphere (Twohy et al., 2010; Stith et al., 2011). For RF03 plume sampling during Periods 1–3, average IN number concentrations, measured at a CFDC processing temperature of −32 °C for condensation/immersion freezing nucleation, ranged from ∼22 L^{-1} to ∼10 L^{-1} (Table 4). Higher IN concentrations (∼30 and ∼47 L^{-1}, respectively) were measured during RF03 Period 4 and within the RF01 plume when the aerosol was processed at a slightly colder temperature (−34 °C). It is not known to what extent these results represent burn variability impacting IN production versus the modestly colder processing temperature that could favor an increase in IN concentration (Möhler et al., 2007). Overall, IN concentrations within the smoke plumes were enhanced compared to background concentrations of ∼6–8 L^{-1} for RF01 and ∼4–6 L^{-1} for RF03.

During all plume sampling, the maximum observed IN/CN ratio (0.008 %) was <0.01 %, estimated by Petters et al. (2009b) as likely to strongly perturb IN concentrations on a regional scale. IN/N$_{>0.1}$ ratios were also less than 0.01 % with IN/N$_{>0.5}$ ratios of ∼0.03–0.07 % and ∼0.2–2 % for CFDC measurements at −32 °C and −34 °C, respectively. Previous laboratory measurements of immersion/condensation freezing of sagebrush combustion aerosols at −30 °C showed a IN/CN ratio below 0.0025 % for five out of seven samples, with a ratio of 0.25 % for two out of seven samples (Petters et al., 2009b), consistent with the ratios measured herein. Considering plume 0.1–1.0 μm unreacted mineral dust number fractions, measured by the A-ATOFMS, of <0.4 % and activation of ∼6–20 % of mineral dust as ice nuclei (Field et al., 2006; Prenni et al., 2009), an IN/N$_{>0.1}$ fraction of <0.08 % would be predicted, suggesting that mineral dust cannot be ruled out as the source of IN. Therefore, measurements are still needed to isolate the specific composition of IN within biomass burning plumes, as discussed by Twohy et al. (2010).

Across five wave cloud research flights during the ICE-L field campaign, Twohy et al. (2010) observed positive correlations between IN concentrations and the number concentrations of soot and biomass burning particle types. The IN concentrations measured within the smoke plumes differ from those predicted by the parameterization of DeMott et al. (2010) (Table 4), which is based a multi-project ambient air compilation and utilizes temperature and the fraction of particles >0.5 μm. This is likely due to the fact that

Table 4. CCN number concentrations are shown (with standard deviations), as well as the fraction of CN (>13 nm) activating as CCN, at 0.5 % supersaturation with respect to water; the average CCN/CN value >1 is physically impossible and shows the uncertainty associated with the measurements and time synchronization. Measured IN number concentrations (with 95 % confidence intervals) are shown for immersion/condensation freezing IN at the noted CFDC processing temperatures. IN/IN_{D2010} described the measured IN number concentration divided by that predicted by the parameterization of DeMott et al. (2010). RF03 Periods 1–4 and the RF01 average correspond to approximate aerosol ages of $\sim$2–4 min, $\sim$32–39 min, $\sim$52–62 min, $\sim$81–88 min, and $\sim$17–30 min, respectively.

	$CCN_{0.5\%}$ (cm^{-3})	$CCN_{0.5\%}$/CN	CFDC Temp. (°C)	IN (L^{-1})	IN/IN_{D2010}
RF03 Period 1	15 318 (2508)	1.12 (0.26)	−31.5	22 (9)	0.21 (0.09)
RF03 Period 2	3005 (73)	0.59 (0.03)	−31.7	16 (8)	0.11 (0.05)
RF03 Period 3	1780 (128)	0.58 (0.06)	−32.2	10 (4)	0.07 (0.03)
RF03 Period 4	350 (12)	0.111 (0.003)	−34.2	30 (12)	0.29 (0.12)
RF01 Average	852 (86)	0.28 (0.02)	−33.5	47 (9)	2.9 (0.6)

the compositions of >500 nm particles in biomass burning plumes are representative of a specific source rather than the average ambient free troposphere (DeMott et al., 2010; Pratt and Prather, 2010).

4 Conclusions

As a major source of aerosols, biomass burning emissions significantly impact global direct radiative forcing and cloud properties (Forster et al., 2007). Given predicted increases in wildfires, particularly in the western United States (Westerling et al., 2006; Spracklen et al., 2009), it is important to understand the physical and chemical properties of biomass burning aerosols, as well as their links to optical and cloud properties (Reid et al., 2005b). Prescribed fires provide the opportunity for a detailed characterization of both burn conditions and consequent emissions in a real-world setting, combining the advantages of studying wildfires and laboratory fires. During ICE-L, the smoke plumes of two Wyoming BLM prescribed burns were intercepted aboard the NCAR/NSF C-130 aircraft. While most airborne plume studies have focused on large fires (e.g. Capes et al., 2008; Yokelson et al., 2009), this study examined two relatively small prescribed burns, characterized primarily by live mountain big sagebrush combustion, with particle aging examined in detail. The chemical composition of the biomass burning particles was investigated in detail utilizing a unique suite of real-time aerosol instrumentation, measuring size-resolved single-particle chemical composition, size-resolved non-refractory mass concentrations, and black carbon mass concentrations. For one plume, the chemical composition was monitored in real-time for smoke particle aging from $\sim$2 min to $\sim$2 h. This work contributes to understanding the chemical composition and mixing state of biomass burning aerosols during aging from emission, using high time resolution measurements to bridge the gap between fresh and aged smoke particles, highlighted in a review by Reid et al. (2005b) as being a major need.

After $\sim$2–4 min of aging, the fresh biomass burning particles were primarily internal mixtures of organic carbon, elemental carbon, potassium chloride, and potassium sulfate. The submicron smoke particles consisted primarily of organics by mass, with an increased fraction of oxidized organics with aging, coincident with the increased presence of dicarboxylic acids. Significantly, nitrate and sulfate were internally mixed with 100 % of the fresh biomass burning particles, despite minor mass fractions, showing hygroscopic material present from the point of emission. Few fresh biomass burning particles by number were internally mixed with ammonium, consistent with the low ammonium mass fraction. Excess black carbon mass concentrations were correlated throughout the plumes with excess CO concentrations consistent with dilution. The mass fractions of ammonium, sulfate, and nitrate increased with aging and resulted in acidic particles, with both nitric acid and sulfuric acid present. Future work should focus on characterizing the partitioning and oxidation of organics during plume aging and dilution. CCN measurements at 0.5 % supersaturation with respect to water suggested activation of all particles >100 nm throughout the smoke plumes, confirming the high CCN activity of these freshly emitted particles. For immersion/condensation freezing, IN measurements at −32 °C suggested activation of $\sim$0.03–0.07 % of particles >500 nm. Mineral dust may be the source of the measured IN concentrations; however, future laboratory and ambient measurements are needed to specifically target and fully characterize the specific smoke plume particles acting as IN, since wildfires can be a significant source of IN (Petters et al., 2009b; Twohy et al., 2010).

References

Aiken, A. C., DeCarlo, P. F., Kroll, J. H., Worsnop, D. R., Huff-
man, J. A., Docherty, K. S., Ulbrich, I. M., Mohr, C., Kimmel,
J. R., Sueper, D., Sun, Y., Zhang, Q., Trimborn, A., Northway,
M., Ziemann, P. J., Canagaratna, M. R., Onasch, T. B., Alfarra,
M. R., Prévôt, A. S. H., Dommen, J., Duplissy, J., Metzger,
A., Baltensperger, U., and Jimenez, J. L.: O/C and OM/OC ra-
tios of primary, secondary, and ambient organic aerosols with
high-resolution time-of-flight aerosol mass spectrometry, Envi-
ron. Sci. Technol., 42, 4478–4485, 2008.

Alfarra, M. R., Prevot, A. S. H., Szidat, S., Sandradewi, J., Weimer,
S., Lanz, V. A., Schreiber, D., Mohr, M., and Baltensperger, U.:
Identification of the mass spectral signature of organic aerosols
from wood burning emissions, Environ. Sci. Technol., 41, 5770–
5777, 2007.

Andreae, M. O. and Rosenfeld, D.: Aerosol-cloud-precipitation
interactions. Part 1. The nature and sources of cloud-active
aerosols, Earth-Sci. Rev., 89, 13–41, 2008.

Bahreini, R., Dunlea, E. J., Matthew, B. M., Simons, C., Docherty,
K. S., DeCarlo, P. F., Jimenez, J. L., Brock, C. A., and Middle-
brook, A. M.: Design and operation of a pressure-controlled in-
let for airborne sampling with an aerodynamic aerosol lens, Aerosol
Sci. Technol., 42, 465–471, 2008.

Baumgardner, D., Kok, G. L., and Raga, G. B.: On the diurnal
variability of particle properties related to light absorbing carbon
in Mexico City, Atmos. Chem. Phys., 7, 2517-2526, 2007,
http://www.atmos-chem-phys.net/7/2517/2007/.

Baumgardner, D., Subramanian, R., Twohy, C., Stith, J.,
and Kok, G.: Scavenging of black carbon by ice crystals
over the northern Pacific, Geophys. Res. Lett., 35, L22815,
doi:10.1029/2008GL035764, 2008.

Bhave, P. V., Allen, J. O., Morrical, B. D., Fergenson, D. P., Cass,
G. R., and Prather, K. A.: A field-based approach for determin-
ing ATOFMS instrument sensitivities to ammonium and nitrate,
Environ. Sci. Technol., 36, 4868–4879, 2002.

Cahill, C. F., Cahill, T. A., and Perry, K. D.: The size- and time-
resolved composition of aerosols from a sub-Arctic boreal forest
prescribed burn, Atmos. Environ., 42, 7553–7559, 2008.

Capes, G., Johnson, B., McFiggans, G., Williams, P. I., Haywood,
J., and Coe, H.: Aging of biomass burning aerosols over West
Africa: Aircraft measurements of chemical composition, micro-
physical properties, and emission ratios, J. Geophys. Res., 113,
D00C15, doi:10.1029/2008JD009845, 2008.

Carrico, C. M., Petters, M. D., Kreidenweis, S. M., Sullivan, A. P.,
McMeeking, G. R., Levin, E. J. T., Engling, G., Malm, W. C., and

Collett, J. L.: Water uptake and chemical composition of fresh
aerosols generated in open burning of biomass, Atmos. Chem.
Phys., 10, 5165–5178, doi:10.5194/acp-10-5165-2010, 2010.

Chand, D., Wood, R., Anderson, T. L., Satheesh, S. K., and Charl-
son, R. J.: Satellite-derived direct radiative effect of aerosols de-
pendent on cloud cover, Nature Geosci., 2, 181–184, 2009.

Chen, L.-W. A., Moosmüller, H., Arnott, W. P., Chow, J. C., Wat-
son, J. G., Susott, R. A., Babbitt, R. E., Wold, C. E., Lincoln,
E. N., and Hao, W. M.: Emissions from laboratory combustion
of wildland fuels: Emission factors and source profiles, Environ.
Sci. Technol., 41, 4317–4325, 2007.

Clarke, A., McNaughton, C., Kapustin, V., Shinozuka, Y., Howell,
S., Dibb, J., Zhou, J., Anderson, B., Brekhovskikh, V., Turner,
H., and Pinkerton, M.: Biomass burning and pollution aerosol
over North America: Organic components and their influence on
spectral optical properties and humidification response, J. Geo-
phys. Res., 112, D12S18, doi:10.1029/2006JD007777, 2007.

Crutzen, P. J., Lawrence, M. G., and Pöschl, U.: On the background
photochemistry of tropospheric ozone, Tellus, 51A-B, 123–146,
1999.

DeCarlo, P. F., Dunlea, E. J., Kimmel, J. R., Aiken, A. C., Sueper,
D., Crounse, J., Wennberg, P. O., Emmons, L., Shinozuka, Y.,
Clarke, A., Zhou, J., Tomlinson, J., Collins, D. R., Knapp, D.,
Weinheimer, A. J., Montzka, D. D., Campos, T., and Jimenez,
J. L.: Fast airborne aerosol size and chemistry measurements
above Mexico City and Central Mexico during the MILAGRO
campaign, Atmos. Chem. Phys., 8, 4027–4048, doi:10.5194/acp-
8-4027-2008, 2008.

DeMott, P. J., Prenni, A. J., Liu, X., Kreidenweis, S. M., Petters,
M. D., Twohy, C. H., Richardson, M. S., Eidhammer, T., and
Rogers, D. C.: Predicting global atmospheric ice nuclei distribu-
tions and their impacts on climate, Proc. Natl. Acad. Sci. USA,
107, 11217–11222, 2010.

Denkenberger, K. A., Moffet, R. C., Holecek, J. C., Rebotier, T. P.,
and Prather, K. A.: Real-time, single-particle measurements of
oligomers in aged ambient aerosol particles, Environ. Sci. Tech-
nol., 41, 5439-5446, 2007.

Donahue, N. M., Robinson, A. L., Stanier, C. O., and Pandis,
S. N.: Coupled partitioning, dilution, and chemical aging of
semivolatile organics, Environ. Sci. Technol., 40, 2635–2643,
2006.

Drewnick, F., Hings, S. S., DeCarlo, P., Jayne, J. T., Gonin, M.,
Fuhrer, K., Weimer, S., Jimenez, J. L., Demerjian, K. L., Bor-
rmann, S., and Worsnop, D. R.: A new time-of-flight aerosol
mass spectrometer (TOF-AMS) – Instrument description and
first field deployment, Aerosol Sci. Technol., 39, 637–658, 2005.

Eagan, R. C., Hobbs, P. V., and Radke, L. F.: Measurements of
cloud condensation nuclei and cloud droplet size distributions in
the vicinity of forest fires, J. Appl. Meteorol., 13, 553–557, 1974.

Eidhammer, T., DeMott, P. J., Prenni, A. J., Petters, M. D., Twohy,
C. H., Rogers, D. C., Stith, J., Heymsfield, A., Wang, Z., Pratt, K.
A., Prather, K. A., Murphy, S. M., Seinfeld, J. H., Subramanian,
R., and Kreidenweis, S. M.: Ice initiation by aerosol particles:
Measured and predicted ice nuclei concentrations versus mea-
sured ice crystal concentrations in an orographic wave cloud, J.
Atmos. Sci., 67, 2417–2436, 2010.

Field, P. R., Mohler, O., Connolly, P., Kramer, M., Cotton, R.,
Heymsfield, A. J., Saathoff, H., and Schnaiter, M.: Some ice
nucleation characteristics of Asian and Saharan desert dust, At-

mos. Chem. Phys., 6, 2991–3006, doi:10.5194/acp-6-2991-2006, 2006.

Forster, P., Ramaswamy, V., Artaxo, P., Berntsen, T., Betts, R., Fahey, D. W., Haywood, J., Lean, J., Lowe, D. C., Myhre, G., Nganga, J., Prinn, R., Raga, G., Schulz, M., and Van Dorland, R.: Changes in Atmospheric Constituents and in Radiative Forcing, in: Climate Change 2007: The Physical Science Basis. Contribution of Working Group I to the Fourth Assessment Report of the Intergovernmental Panel on Climate Change, edited by: Solomon, S., Qin, D., Manning, M., Chen, Z., Marquis, M., Averyt, K. B., Tignor, M., and Miller, H. L., Cambridge University Press, New York, NY, 129–234, 2007.

Gao, S., Hegg, D. A., Hobbs, P. V., Kirchstetter, T. W., Magi, B. I., and Sadilek, M.: Water-soluble organic components in aerosols associated with savanna fires in southern Africa: Identification, evolution, and distribution, J. Geophys. Res., 108, 8491, doi:10.1029/2002JD002324, 2003.

Gaudichet, A., Echalar, F., Chatenet, B., Quisefit, J. P., Malingre, G., Cachier, H., Buat-Menard, P., Artaxo, P., and Maenhaut, W.: Trace elements in tropical African savanna biomass burning aerosols, J. Atmos. Chem., 22, 19–39, 1995.

Goode, J. G., Yokelson, R. J., Ward, D. E., Susott, R. A., Babbitt, R. E., Davies, M. A., and Hao, W. M.: Measurements of excess O_3, CO_2, CO, CH_4, C_2H_4, C_2H_2, HCN, NO, NH_3, HCOOH, CH_3COOH, HCHO, and CH_3OH in 1997 Alaskan biomass burning plumes by airborne Fourier transform infrared spectroscopy (AFTIR), J. Geophys. Res., 105, 22147–22166, 2000.

Grieshop, A. P., Donahue, N. M., and Robinson, A. L.: Laboratory investigation of photochemical oxidation of organic aerosol from wood fires 2: analysis of aerosol mass spectrometer data, Atmos. Chem. Phys., 9, 2227–2240, doi:10.5194/acp-9-2227-2009, 2009.

Guyon, P., Frank, G. P., Welling, M., Chand, D., Artaxo, P., Rizzo, L., Nishioka, G., Kolle, O., Fritsch, H., Silva Dias, M. A. F., Gatti, L. V., Cordova, A. M., and Andreae, M. O.: Airborne measurements of trace gas and aerosol particle emissions from biomass burning in Amazonia, Atmos. Chem. Phys., 5, 2989–3002, doi:10.5194/acp-5-2989-2005, 2005.

Hawkins, L. N. and Russell, L. M.: Oxidation of ketone groups in transported biomass burning aerosol from the 2008 Northern California Lightning Series fires, Atmos. Environ., 44, 4142–4154, 2010.

Heald, C. L., Kroll, J. H., Jimenez, J. L., Docherty, K. S., DeCarlo, P. F., Aiken, A. C., Chen, Q., Martin, S. T., Farmer, D. K., and Artaxo, P.: A simplified description of the evolution of organic aerosol composition in the atmosphere, Geophys. Res. Lett., 37, L08803, doi:10.1029/2010GL042737, 2010.

Hennigan, C. J., Sullivan, A. P., Collett, J. L., and Robinson, A. L.: Levoglucosan stability in biomass burning particles exposed to hydroxyl radicals, Geophys. Res. Lett., 37, L09806, doi:10.1029/2010GL043088, 2010.

Hennigan, C. J., Miracolo, M. A., Engelhart, G. J., May, A. A., Presto, A. A., Lee, T., Sullivan, A. P., McMeeking, G. R., Coe, H., Wold, C. E., Hao, W.-M., Gilman, J. B., Kuster, W. C., de Gouw, J., Schichtel, B. A., Collett, J. L., Kreidenweis, S. M., and Robinson, A. L.: Chemical and physical transformations of organic aerosol from the photo-oxidation of open biomass burning emissions in an environmental chamber, Atmos. Chem. Phys.,

11, 7669–7686, doi:10.5194/acp-11-7669-2011, 2011.

Hobbs, P. V. and Locatelli, J. D.: Ice nuclei from a natural forest fire, J. Appl. Meteorol., 8, 833–834, 1969.

Hobbs, P. V. and Radke, L. F.: Cloud condensation nuclei from a simulated forest fire, Science, 163, 279–280, 1969.

Hobbs, P. V., Sinha, P., Yokelson, R. J., Christian, T. J., Blake, D. R., Gao, S., Kirchstetter, T. W., Novakov, T., and Pilewskie, P.: Evolution of gases and particles from a savanna fire in South Africa, J. Geophys. Res., 108, 8485, doi:10.1029/2002JD002352, 2003.

Hudson, P. K., Murphy, D. M., Cziczo, D. J., Thomson, D. S., de Gouw, J. A., Warneke, C., Holloway, J., Jost, J. R., and Hubler, G.: Biomass-burning particle measurements: Characteristic composition and chemical processing, J. Geophys. Res., 109, D23S27, doi:10.1029/2003JD004398, 2004.

Huffman, J. A., Jayne, J. T., Drewnick, F., Aiken, A. C., Onasch, T., Worsnop, D. R., and Jimenez, J. L.: Design, modeling, optimization, and experimental tests of a particle beam width probe for the Aerodyne aerosol mass spectrometer, Aerosol Sci. Technol., 39, 1143–1163, 2005.

Kessler, S. H., Smith, J. D., Che, D. L., Worsnop, D. R., Wilson, K. R., and Kroll, J. H.: Chemical sinks of organic aerosol: Kinetics and products of the heterogeneous oxidation of erythritol and levoglucosan, Environ. Sci. Technol., 44, 7005–7010, 2010.

Knudsen, J. N., Jensen, P. A., and Dam-Johansen, K.: Transformation and release to the gas phase of Cl, K, and S during combustion of annual biomass, Energy Fuels, 18, 1385–1399, 2004.

Kroll, J. H., Smith, J. D., Che, D. L., Kessler, S. H., Worsnop, D. R., and Wilson, K. R.: Measurement of fragmentation and functionalization pathways in the heterogeneous oxidation of oxidized organic aerosol, Phys. Chem. Chem. Phys., 11, 8005–8014, 2009.

Li, J., Posfai, M., Hobbs, P. V., and Buseck, P. R.: Individual aerosol particles from biomass burning in southern Africa: 2. Compositions and aging of inorganic particles, J. Geophys. Res., 108, 8484, doi:10.1029/2002JD002310, 2003.

Liu, X., Van Espen, P., Adams, F., Cafmeyer, J., and Maenhaut, W.: Biomass burning in Southern Africa: Individual particle characterization of atmospheric aerosols and Savanna fire samples, J. Atmos. Chem., 36, 135–155, 2000.

Matthew, B. M., Middlebrook, A. M., and Onasch, T. B.: Collection efficiencies in an Aerodyne aerosol mass spectrometer as a function of particle phase for laboratory generated aerosols, Aerosol Sci. Technol., 42, 884–898, 2008.

McMeeking, G. R., Kreidenweis, S. M., Baker, S., Carrico, C. M., Chow, J. C., Collett, J. L., Hao, W. M., Holden, A. S., Kirchstetter, T. W., Malm, W. C., Moosmüller, H., Sullivan, A. P., and Wold, C. E.: Emissions of trace gases and aerosols during the open combustion of biomass in the laboratory, J. Geophys. Res., 114, D19210, doi:10.1029/2009JD011836, 2009.

Möhler, O., DeMott, P. J., Vali, G., and Levin, Z.: Microbiology and atmospheric processes: the role of biological particles in cloud physics, Biogeosciences, 4, 1059–1071, doi:10.5194/bg-4-1059-2007, 2007.

Moteki, N. and Kondo, Y.: Effects of mixing state on black carbon measurements by laser-induced incandescence, Aerosol Sci. Technol., 41, 398–417, 2007.

Moteki, N., Kondo, Y., Miyazaki, Y., Takegawa, N., Komazaki, Y., Kurata, G., Shirai, T., Blake, D. R., Miyakawa, T., and Koike, M.: Evolution of mixing state of black carbon particles: Aircraft measurements over the western Pacific in March 2004, Geophys.

Res. Lett., 34, L11803, doi:10.1029/2006GL028943, 2007.

Murphy, S. M., Agrawal, H., Sorooshian, A., Padró, L. T., Gates, H., Hersey, S., Welch, W. A., Jung, H., Miller, J. W., Cocker, D. R., Nenes, A., Jonsson, H. H., Flagan, R. C., and Seinfeld, J. H.: Comprehensive simultaneous shipboard and airborne characterization of exhaust from a modern container ship at sea, Environ. Sci. Technol., 43, 4626–4640, 2009.

Park, R. J., Jacob, D. J., and Logan, J. A.: Fire and biofuel contributions to annual mean aerosol mass concentrations in the United States, Atmos. Environ., 41, 7389–7400, 2007.

Petters, M. D., Carrico, C. M., Kreidenweis, S. M., Prenni, A. J., DeMott, P. J., Collett, J. L., and Moosmüller, H.: Cloud condensation nucleation activity of biomass burning aerosol, J. Geophys. Res., 114, D22205, doi:10.1029/2009JD012353, 2009a.

Petters, M. D., Parsons, M. T., Prenni, A. J., DeMott, P. J., Kreidenweis, S. M., Carrico, C. M., Sullivan, A. P., McMeeking, G. R., Levin, E., Wold, C. E., Collett, J. L., and Moosmuller, H.: Ice nuclei emissions from biomass burning, J. Geophys. Res., 114, D07209, doi:10.1029/2008JD011532, 2009b.

Pósfai, M., Simonics, R., Li, J., Hobbs, P. V., and Buseck, P. R.: Individual aerosol particles from biomass burning in southern Africa: 1. Compositions and size distributions of carbonaceous particles, J. Geophys. Res., 108, 8483, doi:10.1029/2002JD002291, 2003.

Pratt, K. A., Mayer, J. E., Holecek, J. C., Moffet, R. C., Sanchez, R. O., Rebotier, T. P., Furutani, H., Gonin, M., Fuhrer, K., Su, Y., Guazzotti, S., and Prather, K. A.: Development and characterization of an aircraft aerosol time-of-flight mass spectrometer, Anal. Chem., 81, 1792–1800, 2009.

Pratt, K. A. and Prather, K. A.: Aircraft measurements of vertical profiles of aerosol mixing states, J. Geophys. Res., 115, D11305, doi:10.1029/2009JD013150, 2010.

Prenni, A. J., Petters, M. D., Kreidenweis, S. M., Heald, C. L., Martin, S. T., Artaxo, P., Garland, R. M., Wollny, A. G., and Pöschl, U.: Relative roles of biogenic emissions and Saharan dust as ice nuclei in the Amazon basin, Nature Geosci., 2, 402–405, 2009.

Pueschel, R. F. and Langer, G.: Sugar cane fires as a source of ice nuclei in Hawaii, J. Appl. Meteorol., 12, 549–551, 1973.

Reid, J. S., Eck, T. F., Christopher, S. A., Koppmann, R., Dubovik, O., Eleuterio, D. P., Holben, B. N., Reid, E. A., and Zhang, J.: A review of biomass burning emissions part III: intensive optical properties of biomass burning particles, Atmos. Chem. Phys., 5, 827–849, doi:10.5194/acp-5-827-2005, 2005a.

Reid, J. S., Koppmann, R., Eck, T. F., and Eleuterio, D. P.: A review of biomass burning emissions part II: Intensive physical properties of biomass burning particles, Atmos. Chem. Phys., 5, 799–825, doi:10.5194/acp-5-799-2005, 2005b.

Roberts, G. C. and Nenes, A.: A continuous-flow streamwise thermal-gradient CCN chamber for atmospheric measurements, Aerosol Sci. Technol., 39, 206–221, 2005.

Rogers, D. C., DeMott, P. J., Kreidenweis, S. M., and Chen, Y.: A continuous-flow diffusion chamber for airborne measurements of ice nuclei, J. Atmos. Ocean. Technol., 18, 725–741, 2001.

Schneider, J., Weimer, S., Drewnick, F., Borrmann, S., Helas, G., Gwaze, P., Schmid, O., Andreae, M. O., and Kirchner, U.: Mass spectrometric analysis and aerodynamic properties of various types of combustion-related aerosol particles, Int. J. Mass Spectrom., 258, 37–49, 2006.

Schwarz, J. P., Gao, R. S., Fahey, D. W., Thomson, D. S., Watts, L. A., Wilson, J. C., Reeves, J. M., Darbeheshti, M., Baumgardner, D. G., Kok, G. L., Chung, S. H., Schulz, M., Hendricks, J., Lauer, A., Kärcher, B., Slowik, J. G., Rosenlof, K. H., Thompson, T. L., Langford, A. O., Loewenstein, M., and Aikin, K. C.: Single-particle measurements of midlatitude black carbon and light-scattering aerosols from the boundary layer to the lower stratosphere, J. Geophys. Res., 111, D16207, doi:10.1029/2006JD007076, 2006.

Silva, P. J., Liu, D. Y., Noble, C. A., and Prather, K. A.: Size and chemical characterization of individual particles resulting from biomass burning of local Southern California species, Environ. Sci. Technol., 33, 3068–3076, 1999.

Simoneit, B. R. T., Schauer, J. J., Nolte, C. G., Oros, D. R., Elias, V. O., Fraser, M. P., Rogge, W. F., and Cass, G. R.: Levoglucosan, a tracer for cellulose in biomass burning and atmospheric particles, Atmos. Environ., 33, 173–182, 1999.

Spencer, M. T., and Prather, K. A.: Using ATOFMS to determine OC/EC mass fractions in particles, Aerosol Sci. Technol., 40, 585–594, 2006.

Spracklen, D. V., Mickley, L. J., Logan, J. A., Hudman, R. C., Yevich, R., Flannigan, M. D., and Westerling, A. L.: Impacts of climate change from 2000 to 2050 on wildfire activity and carbonaceous aerosol concentrations in the western United States, J. Geophys. Res., 114, D20301, doi:10.1029/2008JD010966, 2009.

Stith, J. L., Radke, L. F., and Hobbs, P. V.: Particle emissions and the production of ozone and nitrogen oxides from the burning of forest slash, Atmos. Environ., 15, 73–82, 1981.

Stith, J. L., Twohy, C. H., DeMott, P. J., Baumgardner, D., Campos, T., Gao, R., and Anderson, J.: Observations of ice nuclei and heterogeneous freezing in a Western Pacific extratropical storm, Atmos. Chem. Phys., 11, 6229–6243, doi:10.5194/acp-11-6229-2011, 2011.

Subramanian, R., Roden, C. A., Boparai, P., and Bond, T. C.: Yellow beads and missing particles: Trouble ahead for filter-based absorption measurements, Aerosol Sci. Technol., 41, 630–637, 2007.

Subramanian, R., Kok, G. L., Baumgardner, D., Clarke, A., Shinozuka, Y., Campos, T. L., Heizer, C. G., Stephens, B. B., de Foy, B., Voss, P. B., and Zaveri, R. A.: Black carbon over Mexico: the effect of atmospheric transport on mixing state, mass absorption cross-section, and BC/CO ratios, Atmos. Chem. Phys., 10, 219–237, doi:10.5194/acp-10-219-2010, 2010.

Sullivan, A. P., Holden, A. S., Patterson, L. A., McMeeking, G. R., Kreidenweis, S. M., Malm, W. C., Hao, W. M., Wold, C. E., and Collett, J. L.: A method for smoke marker measurements and its potential application for determining the contribution of biomass burning from wildfires and prescribed fires to ambient $PM_{2.5}$ organic carbon, J. Geophys. Res., 113, D22302, doi:10.1029/2008JD010216, 2008.

Sullivan, R. C. and Prather, K. A.: Investigations of the diurnal cycle and mixing state of oxalic acid in individual particles in Asian aerosol outflow, Environ. Sci. Technol., 41, 8062–8069, 2007.

Twohy, C. H., DeMott, P. J., Pratt, K. A., Subramanian, R., Kok, G. L., Murphy, S. M., Lersch, T., Prather, K. A., Seinfeld, J. H., Heymsfield, A. J., and Wang, Z.: Relationships of biomass burning aerosols to ice in orographic wave clouds, J. Atmos. Sci., 67, 2437–2450, 2010.

Weimer, S., Alfarra, M. R., Schreiber, D., Mohr, M., Prévôt, A. S. H., and Baltensperger, U.: Organic aerosol mass spectral

signatures from wood-burning emissions: Influence of burning conditions and wood type, J. Geophys. Res., 113, D10304, doi:10.1029/2007JD009309, 2008.

Westerling, A. L., Hidalgo, H. G., Cayan, D. R., and Swetnam, T. W.: Warming and earlier spring increase western U.S. forest wildfire activity, Science, 313, 940–943, 2006.

Wiedinmyer, C. and Hurteau, M. D.: Prescribed fire as a means of reducing forest carbon emissions in the western United States, Environ. Sci. Technol., 44, 1926–1932, 2010.

Yao, X., Rehbein, P. J. G., Lee, C. J., Evans, G. J., Corbin, J., and Jeong, C.-H.: A study on the extent of neutralization of sulphate aerosol through laboratory and field experiments using an ATOFMS and a GPIC, Atmos. Environ., 45, 6251–6256, 2011.

Yokelson, R. J., Crounse, J. D., DeCarlo, P. F., Karl, T., Urbanski, S., Atlas, E., Campos, T., Shinozuka, Y., Kapustin, V., Clarke, A. D., Weinheimer, A., Knapp, D. J., Montzka, D. D., Holloway, J., Weibring, P., Flocke, F., Zheng, W., Toohey, D., Wennberg, P. O., Wiedinmyer, C., Mauldin, L., Fried, A., Richter, D., Walega, J., Jimenez, J. L., Adachi, K., Buseck, P. R., Hall, S. R., and Shetter, R.: Emissions from biomass burning in the Yucatan, Atmos. Chem. Phys., 9, 5785–5812, doi:10.5194/acp-9-5785-2009, 2009.

Zhang, Q., Jimenez, J. L., Worsnop, D. R., and Canagaratna, M.: A case study of urban particle acidity and its influence on secondary organic aerosol, Environ. Sci. Technol., 41, 3213–3219, 2007.